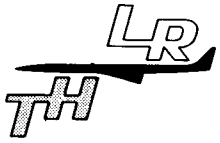

DELFT UNIVERSITY OF TECHNOLOGY

DEPARTMENT OF AEROSPACE ENGINEERING

Report LR-326

ON THE DESIGN OF SOME AIRFOILS FOR SAILPLANE APPLICATION

by

L.M.M. Boermans
H.J.W. Selen

Presented at the XVIIth OSTIV Congress
Paderborn, West-Germany, 1981

DELFT - THE NETHERLANDS

April 1981

DELFT UNIVERSITY OF TECHNOLOGY

DEPARTMENT OF AEROSPACE ENGINEERING

Report LR-326

ON THE DESIGN OF SOME AIRFOILS FOR SAILPLANE APPLICATION

by

L.M.M. Boermans
H.J.W. Selen

Presented at the XVIIth OSTIV Congress
Paderborn, West-Germany, 1981

DELFT - THE NETHERLANDS

April 1981

1. Introduction

At the Delft University of Technology Low Speed Laboratory (LSL) an investigation was conducted to design and test some new airfoils for the wing of a Standard Class sailplane. To avoid building a new wing the airfoils were designed such that just by adding material to the surface an existing wing could be modified and tested in flight. For this purpose, the ASW-19B was selected, fig. 1, mainly because of its relatively thin wing. The manufacturer Alexander Schleicher Segelflugzeugbau was willing to participate in this investigation and provided two wing test segments used for windtunnel experiments as well as a new sailplane which was flight tested before and after the wing modification.

This paper describes the considerations, tests and results of this research. Several subjects are discussed successively:

- Windtunnel experiments on an inner wing and an outer wing segment are described, yielding information about the quality of the actual airfoils achieved in serial production, as well as the quality of the LSL airfoil analysis and design computer program.
- The characteristics of several modern airfoils used in Standard Class sailplanes are analyzed. Typical differences in characteristics, both in case of a smooth surface and in case of a rough leading edge, are clarified.
- Much attention has been given to the problem of leading edge contamination by insects. Insect impact patterns, gathered in flight, show some typical airfoil related differences. Windtunnel measurements with real insect remains on a wing segment and with a well-known simulated bug pattern reveal great differences in drag characteristics.
- A brief discussion is given of the application of pneumatic turbulators, a technique to reduce the drag of an airfoil, rediscovered by Horstmann and Quast, DFVLR Braunschweig, and extensively tested at LSL Delft.

Based on the experience gained in these investigations, two airfoils were designed (for the inner wing respectively the tip of the wing) by utilizing the computer program mentioned before. The inner wing test segment was modified accordingly and tested in the LSL windtunnel.

Next the wing of the ASW-19B sailplane was modified. Flight performance measurements were performed by DFVLR Braunschweig before and after the wing modification. The improvement is, although not yet fully analyzed, most satisfying.

2. Windtunnel measurements on two segments of the ASW-19B wing

At the Delft University of Technology Low Speed Laboratory (LSL) an investigation was conducted to determine the aerodynamic characteristics of two segments of the ASW-19B wing, ref. 1. The wing design and the position of the test segments are shown in fig. 2. The segments are situated approximately in the middle of the inner and outer wing. The inner wing segment was obtained from a wing used for static strength tests, and the outer wing segment was specially built for the present windtunnel tests in the mould. Comparison shows that the actual airfoil shapes measured at the segment mid-spans are about 1.2% chord thicker than the local design shapes, fig. 3.

The wing segments were placed vertically in the windtunnel test section, which is 1.80 m. wide and 1.25 m. high. For further details the reader should consult ref. 1.

For accurate pressure distribution measurements the inner wing segment was provided with 107 pressure orifices (nominal diameter 0,4 mm.) situated in the mid-span chord. A selection of measured pressure distributions at $Re = 1.5 \times 10^6$ is presented in fig. 4, and fig. 5 shows the aerodynamic characteristics. Excessive forces restricted the measurements to $C_l < 1.15$ at $Re = 3 \times 10^6$.

By using a stethoscope, the oilfilm technique and from pressure distributions the following observations were made. On the lower surface a laminar separation bubble is present at all investigated Reynolds numbers and angles of attack above approximately -3°. At the lower end of the low-drag bucket, when transition on the lower surface moves rapidly forward at decreasing angle of attack, no bubbles were found on the lower surface. On the upper surface the bubble is present at angles of attack up to approximately 6°.

At higher angles of attack transition becomes the "normal" instability type (no bubble). It is noted that also in these cases transition is indicated by a hump in the pressure distribution (see fig. 4.2, $\alpha = 8^\circ$, 27% chord upper surface), caused by the jump in boundary layer displacement thickness and hence effective airfoil contour.

Although turbulent separation moves forward rapidly at angles of attack higher than 10°, the pressure distribution develops such as to cause a gradual stall.

The outer wing segment, which had no aileron, was investigated only with respect to flow behaviour and drag characteristics. Calculation showed that due to the taper ratio the greater part of the outer wing has an airfoil more resembling the inner wing airfoil than the tip airfoil. Consequently the test results of the outer wing segment were similar to the inner wing segment results, so there was no need to provide the outer wing segment with pressure orifices. As an example, fig. 6 shows oil-flow patterns, made at a practical situation, where there is the "normal" instability type transition and some trailing edge separation on the upper surface and a quite long laminar separation bubble (11% local chord) on the lower surface.

The characteristics of the actual inner wing airfoil, named FX61-163/ASW-19B, and of the design airfoil FX61-163 were calculated with the LSL airfoil analysis and design computer program as it was available at the time the measurements took place. The results, presented in ref. 1, indicated a slightly higher drag coefficient for the actual airfoil, while the lift versus angle of attack curves coincided. However, there was a striking discrepancy between the calculated and the measured lift versus angle of attack curve in that the measured lift was about $\Delta c_l = 0.15$ lower than the calculated lift. This clearly demonstrated the importance to take into account the effect of the curvature of the wake (which acts as a fluid flap). A description of the procedure which has been incorporated in the computer program is given in ref. 2.
It is clear that the computer program - although not perfect in every detail as will be shown, so that windtunnel measurements remained necessary for verification - was an indispensable tool in the design process which ultimately led to the improved airfoils.

3. Analysis of some airfoil characteristics

A comparison of the characteristics of the airfoils which are commonly used in modern Standard Class high performance sailplanes, supplemented with some calculated results, clarify some typical features.

In general, the Wortmann airfoils designed after 1964 (as FX S02-196 and FX 66-S-196V1) have lower drag coefficients at high lift coefficients than earlier designs (as FX 61-163 and FX 61-184), as shown by the examples in fig. 7, taken from ref. 3.

The pressure distribution of the later types is such that in the low drag range of lift coefficients transition on both sides of the airfoil stays near a particular chord position. The upper end of the low drag bucket is pronounced and coincides with the maximum lift coefficient: i.e. when transition moves forward suddenly due to the development of a pressure peak on the airfoil nose, separation of the turbulent boundary layer at the rear of the airfoil follows.

On the earlier designs the pressure distribution develops such that transition on the upper surface moves steadily in forward direction at increasing angle of attack, thus increasing the drag (and decreasing the lift curve slope). When transition approaches the airfoil nose the turbulent boundary layer starts to separate at the trailing edge.

On the well-known Eppler airfoil E603 transition and turbulent separation move forward steadily at the high angles of attack (instead of suddenly as on the "after 1964" Wortmann airfoils), thus rounding off just the upper edge of the low drag bucket.

In order to get some qualitative information about the effects of a rough leading edge - the next chapter will discuss the insect contamination problem in more detail - the characteristics of the airfoils previously mentioned were calculated, at practical combinations of lift coefficient and Reynolds number, with the assumption of a turbulent boundary layer from 5% chord on both sides of the airfoil.

In addition to an almost doubling of the upper and lower surface drag contributions at attached flow conditions, the calculations indicated serious separation problems for the upper surface flow of the E603 and "after 1964" Wortmann airfoils, and no such problems for the earlier Wortmann designs. At the newer types the turbulent boundary layer is not able to overcome the pressure gradients on the rear part of the airfoil up to the trailing edge.

Windtunnel experience at LSL with roughness on the nose of FX 66-S-196V1 (as already noticed in ref. 4) and E603 (used in the present research

program as described in ref. 2), as well as the results presented in the next chapter confirmed these predictions.

4. Leading edge contamination by insects

From gliding practice the serious degradation of performance (increased sink rate, increased stalling speed and sometimes bad stalling behaviour) caused by insect contamination of the wing leading edge or by collection of rain, is well-known. In order to investigate whether measures could be taken to alleviate these problems by proper airfoil design, some flight experiments and windtunnel tests were carried out. Main results of this research, which is still going on, will be described.

In order to establish whether there is a relation between airfoil shape and insect impact pattern, as suggested in ref. 5, flights were carried out with seven different sailplanes, flying simultaneously most of the time, and gathering insects on sheets of self-adhesive matted polyester film attached to the wing. The 0.08 mm. thick and 0.59 m. wide sheets were placed both on the left and on the right inner wing at equal distance from the wing root, covering about the front half of the local wing depth. After the tests the sheets were carefully removed and pinned on frames for transport and further examination. Due to the mat coating the traces of ruptured insects could easily be found.

All sailplanes were winch-launched at Venlo (The Netherlands), sometimes more than once, and their pilots were asked to perform a normal local flight. Weather circumstances were normal for a sunny day in July and small cumulus clouds aided in thermal finding: the mean value of the reported climb rates was about 1.5 $^{m}/s$. Fortunately, the density of the aerial insect population, which consisted almost exclusively of Aphides, was high; more than 3000 insects were captured. The long wet period preceding the test day may have contributed to this.

Two additional sheets to be used for the windtunnel measurements which will be described, were placed on the left and right wing of an ASW-19B at a spanwise position corresponding to the position of the inner wing test segment (fig. 2) and covering the whole local wing depth. To simulate the surface condition of the clean wing these sheets were painted accordingly. Nevertheless, while no difference could be observed between the different coated sheets, the sheets in general seemed to be a little less contaminated than the wing surfaces adjacent to it (probably the sheets were smoother than the wing surfaces).

Anyhow, since the Aphid is probably the best representative of the great majority of insects, which consist of small and relatively fragile kinds and are therefore most liable to cause insect roughness, the present results

may represent a severe case of insect contamination.
Table 1 lists data and main results of the insect impact measurements. The results for the left and the right wing sheet were put together because they did not show any peculiar difference. Fig. 8 shows the extent of the impacts on the upper and lower surface of the local airfoil shapes. The reason for comparing the fractional chord extent of the impacts is, as elucidated in the Appendix, that this ratio depends (theoretically) on airfoil shape, speed and angle of attack, but not on the absolute size of the airfoil (i.c. chord length). Fig. 9 shows some typical insect impact distributions.
The different relations between speed and angle of attack for the non-flapped and the flapped airfoils - the range of angles of attack for the flapped airfoils is much smaller - as well as the sharp nosed rather flat lower surface of the flapped airfoils cause the great difference in insect impact distribution and extent as given in table 1 and shown in fig. 8 and 9.
With respect to the KA-6CR results it should be mentioned that the pilot, for reasons of staying aloft, never exceeded 110 km/h. Probably the low flight speed has affected the impact pattern (less ruptured insects, shorter impact extent).
No correlation between airfoil thickness and the number of impacts per minute could be established. According to theory, ref. 6, the insects are only slightly deviated by the induced velocity field set up by the airfoil, and hence, less impacts could have been expected on the thinner airfoil. Anyhow, although not all the results of these naturally roughened sheets can be fully explained, it is clear that there is a great difference between impact patterns of flapped and non-flapped airfoils. While at non-flapped airfoils some 55% of the total number of impacts is found on the upper surface and 45% on the lower surface, these figures read roughly 80% and 20% for the flapped airfoil. Apart from the corresponding great difference in the fractional chord extent of the impacts, there is a trend toward a less extended impact pattern for the thinner airfoil.

However, windtunnel measurements, which will be described, revealed that these results with respect to overal leading edge contamination are not crucial.

The thickest insect splatters, which are found on the very leading edge, cause premature transition, while the remains and traces more rearward do not add any contribution to the drag. Comparison of the impact distributions in front of 1% chord and 2½% chord, table 1, shows that for the modern sailplanes (KA-6CR excluded) the relative differences in impact distribution on upper and lower surface for the non-flapped as well as for the flapped airfoils are quite small. Consequently, it was concluded that improvements in airfoil characteristics at present purposes had to come from a proper development of the turbulent boundary layer (at least no separation problems as on the modern airfoils mentioned before).

Windtunnel measurements were performed with the two naturally roughened sheets mentioned before, attached to the inner wing test segment. The lift coefficient was found from the tunnel-wall pressures and the correlation between tunnel-wall pressures and lift coefficient of the clean wing. Mean drag coefficients were obtained from measured drag distributions along 0.15 m. span (staying out of the turbulent wedges which occasionally originated from the rims of the sheets). The onset of turbulent flow was detected by a stethoscope.

In a similar way the aerodynamic characteristics of the inner wing section, but now provided with an artificial "bug pattern", were determined. This bug pattern, consisting of rows of little squares of silver duct tape on the leading edge of the wing, is used in the U.S.A. in measuring the performance of gliders, thus hoping to simulate a fairly severe collection of insects, ref.7. The simulated insects, 0.33 mm. thick and measuring 5 mm. on the sides, were placed each 150 mm. directly on the leading edge, another row in between 25 mm. above the leading edge, and a third row also in between and 13 mm. below the leading edge.

Fig. 10 presents the results for practical combinations of angle of attack and Reynolds number.

While at lift coefficients higher than 0.8, which corresponds to speeds lower than 91 km/h at a wing loading of 32 kgf/m^2, the drag curves of the artificial and real insects coincide, there is a remarkable difference at lower lift coefficients, i.e. the greater part of the speedpolar, where the contribution of the profile drag to the total drag of the sailplane increases with speed.

At negative angle of attack the drag increase due to the real insects is roughly half the increase due to the simulated insects.
With respect to the real insect measurements, the stethoscope revealed that at positive angles of attack the upper surface flow was disturbed by the insects on the airfoil nose (and at angles of attack beyond 6 degrees the area washed by turbulent flow rapidly increased) while the lower surface flow was not disturbed since the location of transition was corresponding to the clean airfoil case. At negative angles of attack it was the reverse; the lower surface flow was disturbed by the insects on the airfoil nose and the upper surface flow showed a position of transition corresponding to the clean airfoil case. At zero angle of attack the height of the insect remains is below the critical roughness height, and no drag increase results.
The left wing sheet was examined in more detail at a Reynolds number of 1.5×10^6. As shown in fig. 11, the range of angles of attack where the insect remains are not, or to a less extent, disturbing the flow is increased. Also shown are the decrease of the lift curve slope and maximum lift coefficient due to the growth of the upper surface boundary layer thickness, which reduces the effective camber. (Although the method to obtain the lift coefficient from wall pressure measurements is not accurate at high angles of attack as shown in fig. 11, the effect of the roughened leading edge is obvious).
A successive removal of the remains behind respectively 2.5% c and 1% c did not yield any change in characteristics at this Reynolds number.
With all the insects removed, the characteristics correspond to the results obtained earlier for the airfoil without sheet.
No stethoscope measurements were performed for the artificial roughness case. However, the drag measurements show that the bugs are located such that there is no situation where none of them disturbe the flow. Moreover, the drag depends very much on the bug pattern (ref. 1). More research is clearly necessary to determine the conditions on the airfoil nose relevant for the insect contamination case and useful in theoretical and experimental work.

5. Drag reduction by pneumatic turbulators

At Delft Low Speed Laboratory an airfoil was extensively tested, HQ 17/14.38, designed by Horstmann and Quast, DFVLR Braunschweig. This airfoil will be applied in the wing of the ASW-22, a new Open Class sailplane (24 m. span) which is being built at Schleicher's factory now. Special feature of this airfoil is the application of pneumatic turbulators, a more detailed discussion on this subject is given in ref. 8.
It is well-known that laminar separation bubbles may spoil the initial conditions of the turbulent boundary layer, thus increasing the drag of an airfoil. Wortmann gave a solution to the problem by using a so called instability region, being a region with a slightly adverse pressure gradient which destabilizes the laminar boundary layer without causing separation, ref. 9. Considering the various combinations of angle of attack and Reynolds number at which the airfoil should have the lowest possible drag it is obvious that this region should be carefully designed.
Another method to decrease drag by avoiding laminar separation bubbles is to disturb the boundary layer in the vicinity of the laminar separation point by blowing air through small orifices periodically spaced in spanwise direction. In this way Pfenninger obtained a drag reduction, for a particular airfoil at a constant angle of attack, which started at $Re = 2 \times 10^6$ and gradually increased with decreasing Reynolds number up to 40% at $Re = 0.33 \times 10^6$ (ref. 10).
Fig. 12 shows, as an example, the drag reduction which was obtained by using such pneumatic turbulators on the lower surface of the HQ 17/14.38 airfoil. Although the pronounced laminar separation bubble is not completely removed in this case, the drag reduction is still up to 10%.
Also shown is the result of the LSL airfoil analysis and design computer program, showing a fair agreement with the measurements except for the prediction of the drag increase due to laminar separation bubbles.
(Meanwhile it has been established that the method which calculates the change in boundary layer characteristics between transition and reattachment has to be improved, and experimental research has been started.)

6. Airfoil design and test results

Based on the experience gained in former studies two airfoils were designed, for the inner wing respectively the tip of the ASW-19B wing. For weight reasons the new airfoils should fit as tightly as possible around the existing one, especially at the aileron (flutter); this puts of course a limitation to the designs. During the design process the effect of calculated changes in airfoil characteristics on the sailplane performance were repeatedly evaluated using the computer program for parametric sailplane performance optimization, described in ref. 11.

First the inner wing airfoil was designed. Fig. 13 shows the new design, named DU 80-176, fitted to the inner wing test segment airfoil. Fig. 14 compares some potential flow pressure distributions, and fig. 15 shows the calculated characteristics at practical combinations of lift coefficient and Reynolds number.

The upper surface was designed for a longer laminar flow extent in case of a clean airfoil, and no separation problems in case of a roughened leading edge. In combination with the lower surface the maximum lift coefficient should be slightly increased.

The lower end of the low drag bucket was determined at $c_l \approx 0.2$ considering the sailplane penetration speeds in relation to practical climb speeds and a margin for vertical air velocity fluctuations during the penetration phase.

Increasing the laminar flow region on the lower surface, while maintaining lift (aft-loading) introduced the danger of pronounced laminar separation bubbles. Here, the use of pneumatic turbulators seemed to be promising. While fixing the position of laminar separation, needed for the application of these turbulators, is easy to obtain through a proper design of the pressure distribution, the desired development of the boundary layer in front of the laminar separation point needed more iterations.

According to stability theory, small harmonic disturbances in the laminar boundary layer become unstable and amplify, the amplitude ratio is expressed by $\frac{a}{a_o} = e^{\sigma_a}$. As soon as they have gained a sufficient amplification, transition occurs. The corresponding amplification factor $\sigma_a = \sigma_{turb}$, however, is a function of the free-stream turbulence and other disturbances such as sound.

Consequently different values of σ_{turb} (and hence different aerodynamic characteristics, in particular drag coefficients) may be valid for a given windtunnel facility and for free flight. A detailed discussion about this phenomenon is given in ref. 1.
The pressure distribution on the lower surface of DU 80-176 was designed such that, at situations near the lower end of the low drag bucket, the amplification factor gradually increases in chordwise direction. The effect is twofold. Due to the controlled movement of the position of transition the drag increases more or less gradually and not suddenly, as calculations indicated for the actual inner wing airfoil, fig. 15. Secondly, at free flight conditions, where σ_{turb} is higher than in the windtunnel situation, the transition position starts to move forward at a lower angle of attack than in the windtunnel, thus extending the low drag range at the lower end. For DU 80-176 this extension would correspond to about 25 km/h in flight speed.
(It is believed that this effect causes the discrepancy which is often found when measured speedpolars - in particular those of sailplanes with flaps - are analyzed by using airfoil data obtained in a windtunnel.)
Finally, it was realized that the lower surface, squeezed out for laminar flow conditions, is not optimal in case of a roughened leading edge. Practice will learn whether maintaining adequate climbing performance will compensate this drawback.

The inner wing test segment was modified to the new airfoil shape, and the windtunnel tests were repeated. Again, the lift coefficient was obtained from the tunnel-wall pressures. The results, shown in fig. 16, as well as oil-flow patterns indicated the existence of pronounced laminar separation bubbles on the lower surface except at situations near the lower end of the low drag bucket at $Re = 3 * 10^6$. At practical combinations of angle of attack and Reynolds number, no bubble was present on the upper surface. The intended lift coefficient at the lower end of the low drag bucket and gradual drag increase below it, as well as a slightly higher maximum lift coefficient (formerly 1.39, now 1.45) were realized.
Next, tests were performed at four practical combinations of lift coefficient and Reynolds number to determine the best location of the

pneumatic turbulators, as well as the air volume flow needed to obtain the lowest drag. Forty pneumatic turbulators, existing of 20 mm. long tubes with 0.6 mm. inner diameter and installed with 16 mm. interspace, were tested at 63, 64, 65 and 67% chord position. (From oil-flow patterns the laminar separation position was detected at 63-64% chord.) By pressurizing the wing test segment the air volume flow was varied from zero up to 150 cm^3/sec. While the results of the 63, 64 and 65% chord position did not differ much (the 65% chord position showed the smoothest drag curve), the 67% chord position was clearly too far rearward. The air volume flow needed to obtain the lowest drag was not critical, the curves showed a flat optimum. A value of 80 cm^3/sec was suitable at the four practical combinations of lift coefficient and Reynolds number.
Fig. 17 shows the characteristics with pneumatic turbulators at 65% chord and an air volume flow of 80 cm^3/sec. At the lower end of the low drag bucket for $Re = 3 \times 10^6$, where the laminar separation bubble in case of not blowing is very small or absent, the pneumatic turbulators do not have any effect. At the remaining situations up to $C_l \approx 1.3$ the drag decrease is dramatic. The effect on lift is negligible.

In fig. 18 the measured characteristics of the new and the original airfoil are compared at practical conditions. While the drag of the new airfoil is slightly higher at $C_l \approx 1.25$ (i.e. insignificant in terms of sailplane drag), the drag decreases to over 10 percent at low lift coefficients, and the maximum lift coefficient is slightly increased. Thus, though the calculated drag (fig. 15) is lower than the measured drag, the predicted trends are in fair agreement with the measurements.
Also shown in fig. 18 are the results where the air volume flow was obtained by means of an open ended forward facing tube (diameter 4 mm.) mounted on the tunnel-wall. The same results, not shown here, were obtained with the air volume flow obtained from 80 orifices (diameter 0.6 mm., equally spaced 8 mm.) drilled at 90% chord of the lower surface, being the location with the highest pressure in the turbulent part of the airfoil.
Finally, fig. 19 shows the results with the simulated bug pattern mentioned before.

The maximum lift coefficient is practically maintained (as intended) and the drag at positive angles of attack is lower than for the original airfoil, fig. 10. However, even when the drag increase due to real insects should be half of the drag increase due to simulated insects at $\alpha < 0^{o}$, the pilot should (as always) be aware of the consequences of flying to fast with contaminated leading edges.

Next the tip airfoil was designed. The considerations were similar to the previous case, with the addition of the severe limitation that the shape of the aileron should not alter. Several attempts resulted in a modification of mainly the lower surface, as shown in fig. 20, thus making the outer wing suitable for the application of pneumatic turbulators. A comparison of potential flow pressure distributions and calculated characteristics is presented in fig. 21 and fig. 22. Again, the estimated effect of free flight conditions on the location of transition could be exploited. This airfoil was not tested in the wind-tunnel.

Since the outer wing is formed by linear lofting, aileron deflections of plus and minus 5 degrees were examined at both the inner wing airfoil and the tip airfoil. No problems are expected, as far as the calculations concern.

7. Sailplane wing modification and flight performance test results

Experience gained with the weight penalty of the modification of the inner wing test segment indicated an increase in minimum wing loading of about 7%. For compensation, considering the climb performance of the unmodified sailplane, the inner wing airfoil was slightly more cambered, yielding a maximum lift coefficient of about 1.47. This airfoil, named DU 80-176V1, and the tip airfoil DU 80-141 were used in modifying the ASW-19B wing.

After removing the white surface coat, the wing was modified by adding respectively foam, a glass-fiber skin, light-weight filling material and finally white surface paint. The correct shape was grinded with the help of 15 templates (for each 0.5 m. span position) and 8 additional nose templates.

Some 870 little tubes (pneumatic turbulators), weighing only 70 grams in total, were installed. Similarly to the windtunnel tests, the air volume flow needed for the pneumatic turbulators was obtained by pressurizing each wing half by means of a nozzle mounted on the streamline cap which covered the aileron actuator. Flight experiments showed that a nozzle diameter of only 6.5 mm. was needed to obtain the right internal wing pressure.

Fig. 23 shows the performance curves of the sailplane before and after the wing modification, as measured by DFVLR, Institut für Flugmechanik, Braunschweig. At the moment of writing the concept of this paper a detailed analysis of the new performance polar, by using the computer program described in ref. 11, has not yet been performed. Anyhow, the improvement is most satisfying, partly even beyond expectation. Not shown is the performance curve obtained with the pneumatic turbulators inactive (covered by tape); the curve coincides with the polar of the unmodified sailplane. Obviously the drag increase due to the pronounced laminar separation bubbles on the lower surface in case of inactive turbulators is equal to the sum of the drag reductions of the improved upper and lower surface in case of active turbulators.

Stalling behaviour is very gentle, and a test with the wing surface entirely wetted in flight by water drained from the DFVLR test sailplane Cirrus revealed no change in minimum flight speed in comparison with the clean wing case.

Acknowledgement

The authors are indebted to the colleagues at the Low Speed Laboratory for their pleasant and valuable support, to Mr. M. Wijnheijmer for performing the windtunnel tests on the outer wing segment, to Mr. H. Werges for the preparations of the windtunnel test segments, to Mr. J. Nieuwland and Mr. M. Jutte for manufacturing the templates, to the Dutch crew which assisted in modifying the wing, to the colleagues at DFVLR Braunschweig for their pleasant cooperation and careful flight performance measurements, and last but not least to the manufacturer of the ASW-19B, Alexander Schleicher Segelflugzeugbau, and its designer Mr. G. Waibel for their most appreciated support and interest.

References

1. Boermans L.M.M.
   Selen H.J.W.
   Wijnheijmer M.L.
   Windtunnel Tests on Two Wing Segments of the ASW-19 Sailplane.
   Memorandum M-379
   Delft University of Technology, Department of Aerospace Engineering, August 1980

2. van Ingen J.L.
   Boermans L.M.M.
   Blom J.J.H.
   Low Speed Airfoil Section Research at Delft University of Technology.
   ICAS-80-10.1 October 1980

3. Althaus D.
   Stuttgarter Profilkatalog I
   Institut für Aero- und Gasdynamik der Universität Stuttgart. 1972

4. Gooden J.H.M.
   Experimental low-speed aerodynamic characteristics of the Wortmann FX 66-S-196V1 Airfoil.
   OSTIV - Publication XV

5. Zacher H.
   Messungen zum Einfluss der Insektenrauhigkeit auf die Flugleistungen.
   Aerokurier 2, 1978

6. Coleman W.S.
   Roughness Due to Insects.
   Boundary Layer and Flow Control, Volume 2
   G.V. Lachmann, ed., Pergamon Press, 1961, pp. 682-747.

7. Johnson R.H.
   A Flight Test Evaluation of the Standard Cirrus B.
   Soaring, March 1976

8. Horstmann K.H.
   Quast A.
   Drag Reduction by Pneumatic Turbulators.
   OSTIV-Congres 1981 Paderborn, West-Germany.

9. Wortmann F.X. Progress in the Design of Low-Drag Airfoils. Boundary Layer and Flow Control, Volume 2 G.V. Lachmann, ed., Pergamon Press, 1961, pp. 748-770.

10. Pfenninger W. Untersuchungen über Reibungsverminderungen an Tragflügeln, insbesondere mit Hilfe von Grenzschichtabsaugung. Mitteilung 13 der ETH, Zürich, 1946

11. Boermans L.M.M. Development of a computer program for parametric sailplane performance optimization. OSTIV Publication XV

12. Head M.R. Transition due to roughness. J.R. Aeron. Soc. Vol. 69, 1965, pp. 344-345

Appendix

In Coleman's comprehensive work with respect to the insect problem, ref. 6, it is shown that in most practical cases - certainly in the present ones - the differential equations which rule the insect trajectory may be solved by assuming that the parameter

$$\mathcal{K} = \frac{1}{2} \cdot c_d \cdot \frac{c}{l} \cdot \frac{\rho_{air}}{\rho_{insect}}$$

is a constant. This parameter links the size, density and drag coefficient of the insect with the size of the airfoil and density of the air. As a result, the trajectory of an insect is independant of the velocity of the approaching airfoil, and impact velocities can be presented in dimensionless form against the fractional chord position, similar to the velocity distribution of an airfoil set at a particular angle of attack.

When the component of the impact velocity normal to the surface is greater than a particular value, termed rupture velocity, the insect will disintegrate and sticks to the surface or leaves a trace. This rupture velocity varies between species.

—Coleman measured in a windtunnel rupture velocities of $10^m/s$ (Aphids), $12^m/s$ (house fly), $14^m/s$ (fruit fly Drosophila)) and $20^m/s$ (Mormoniella, a pupal parasite of the house fly, which has about the same size as an Aphid), while field experiments showed a mean value of $11^m/s$ with possible variations of $1.8^m/s$. Since the extent of the impacts depends on the most fragile insects encountered, the Aphid is most suitable for such experiments.—

From these considerations the interesting conclusions can be drawn that for a particular airfoil and aerial insect population, the roughness height distribution of the remains and the extent of the insect impacts, in terms of fractional chord, depends on speed and angle of attack, but not on the size of the airfoil. The number of impacts is related to the size of the airfoil. Moreover, in ref. 12 it is shown that when the size of an airfoil is increased from chord length c_1 to c_2 and the speed (exactly: the unit Reynolds number U/ν) remains unchanged, the tolerable roughness height increases as $(\frac{c_2}{c_1})^{\frac{1}{4}}$. Thus, doubling the size of an airfoil means an increase in tolerable roughness height of only 19%.

Combining the foregoing arguments lead to some practical conclusions as:

- two wings with similar shape but different size, flying at equal wing loading, are equally sensitive for insect contamination. However, the bigger one may have a higher drag coefficient because of the greater number of insects it captures.
- the taper ratio of a wing with continuous airfoil shape does not influence the local sensitivity of the flow for insect contamination, however the number of insects and in consequence the local drag coefficient may increase towards the wing root.

		NO FLAP				FLAP		
Type		ASW-19B	St. Cirrus	Astir	KA-6CR	Nimbus II	LS-3A	Vega
Wing loading	kgf/m^2	31.7	29	29	22.6	30.6	31.6	31.4
Airfoil		FX61-163	(*)	E 603	NACA 63_2-618→K4	FX67-K-170	FX67-K-170	FX67 K-150
Distance from wing root	m.	1.50	1.50	1.50	3.25	2.65	1.50	1.50
Local chord	m.	0.83	0.81	0.95	0.87	0.84	0.83	0.79
Local thickness	%C	16.3	19.2	19.2	15.8	17.0	17.0	15.0
Flight time	min.	187	230	223	267	195	282	190
Starts		2	1	1	3	1	3	1
Impacts	Total	457	420	455	247	466	613	283
Distribution in	upper	48	56	58	55	84	75	75
% of total	lower	52	44	42	45	16	25	25
Extend in	upper	12	18	16	7	20	19	15
% chord	lower	14	15	16	9	4	5	5
Impacts < 1%C	% total	33	38	37	57	34	35	41
Distribution in	upper	19	23	22	28	24	24	28
% of total	lower	14	15	15	29	10	12	13
Impacts < 2½%C	% total	57	54	55	81	53	54	64
Distribution in	upper	31	32	32	39	38	36	45
% of total	lower	26	22	23	42	15	18	19

(*) FX66S02-196 →FX66-17AII-182

Table 1: Results of insect impact measurements on two sheets of self-adhesive matted polyester film (0.59 m. wide), attached to the left and right wing at equal distance from the wing root.

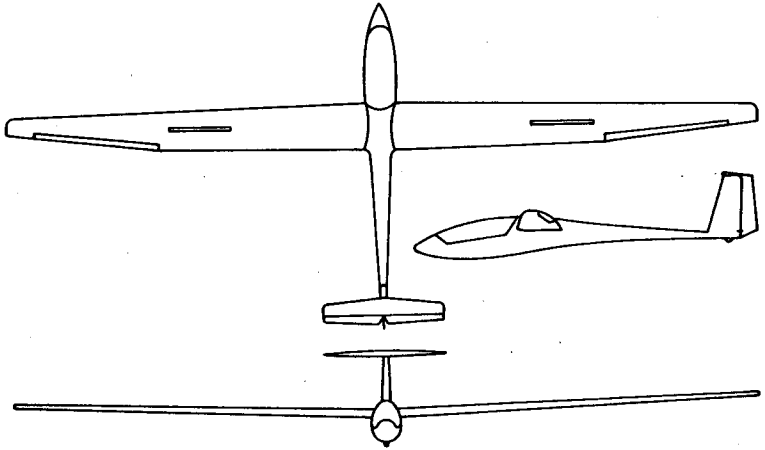

ASW-19B

Wing	
span	15 m
area	11.0 m^2
aspect ratio	20.45
airfoils	FX61-163 (inner wing) FX60-126 (tip)
root chord	0.91 m
tip chord	0.40 m
sweep (0.25 chord)	0^o
twist	0^o inner wing, -2^o tip
Fuselage	
length	6.80 m
breadth	0.63 m
depth	0.81 m
Tail	
hor. tail area	1.10 m^2
hor. tail airfoil	FX71-L-150/30 (12%)
vert. tail area	1.0 m^2
vert. tail airfoil	FX71-L-150/30 (13.5%)
Weight	
empty weight	245 kg
max. useful load	115 kg
max. water ballast	100 kg
all-up weight with ballast	454 kg
wing loading at 85 kg useful load	30 kg/m^2
wing loading at permissible all-up weight	41.3 kg/m^2

Fig. 1: The ASW-19B

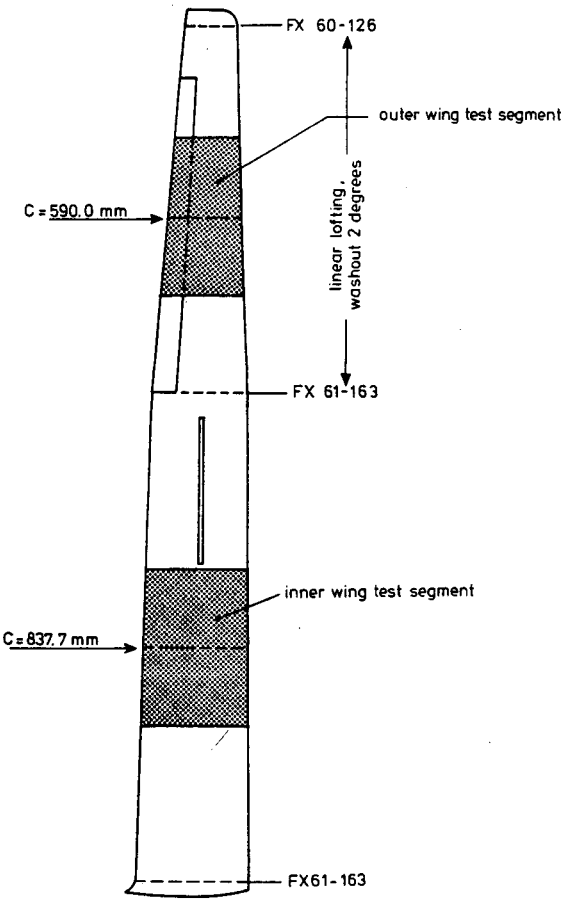

Fig. 2: Position of the test segments in the ASW-19B wing.

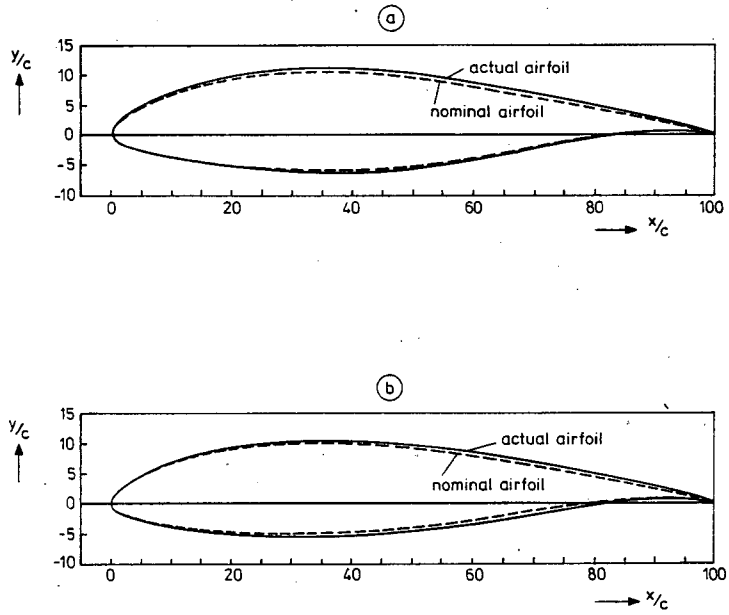

Fig. 3: Actual and nominal airfoil sections at the midspan position of (a) the inner wing test segment and (b) the outer wing test segment.

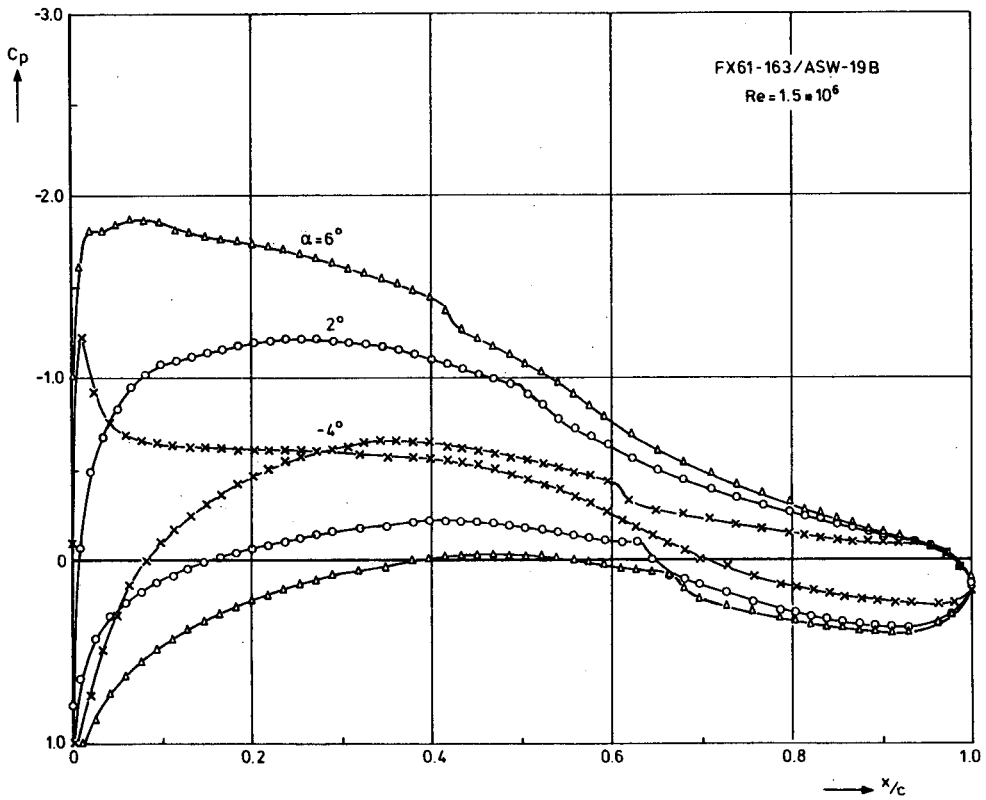

Fig. 4.1: Measured pressure distributions of the inner wing airfoil section.

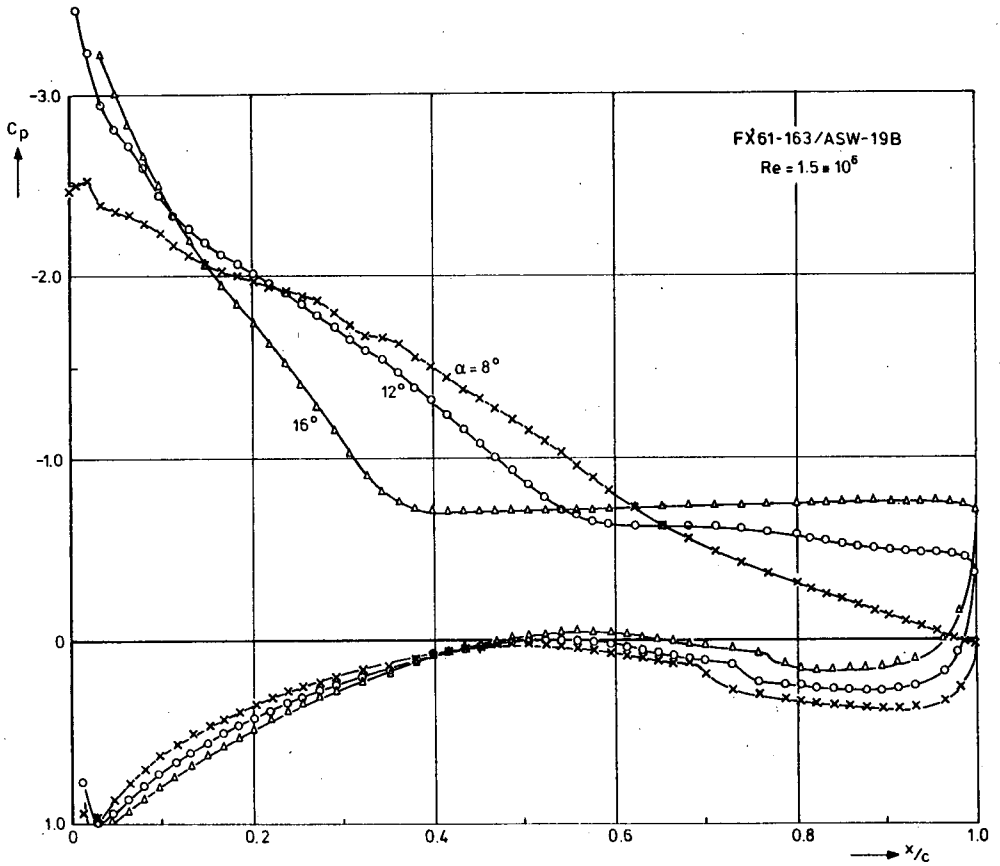

Fig. 4.2: Measured pressure distributions of the inner wing airfoil section.

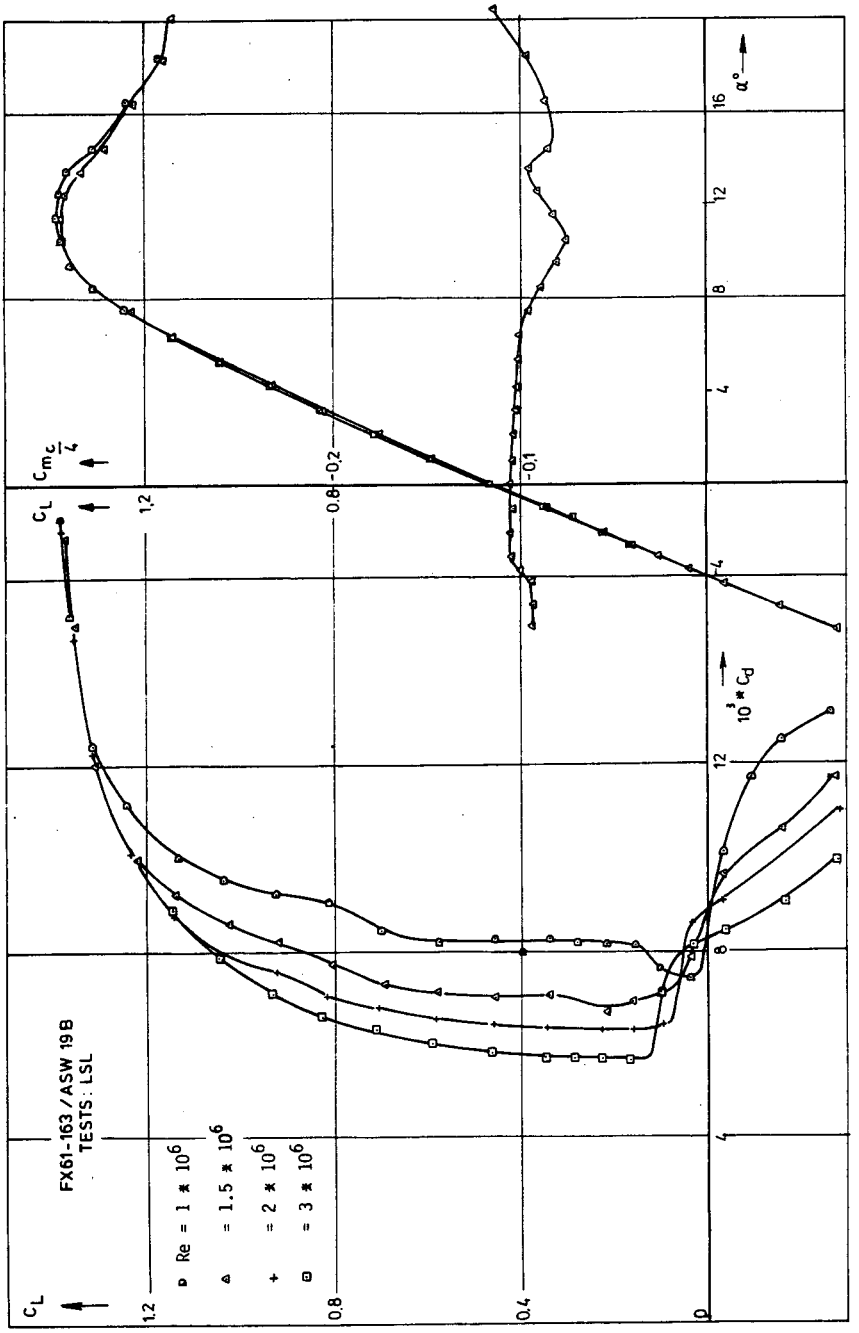

Fig. 5: Measured aerodynamic characteristics of the inner wing airfoil section.

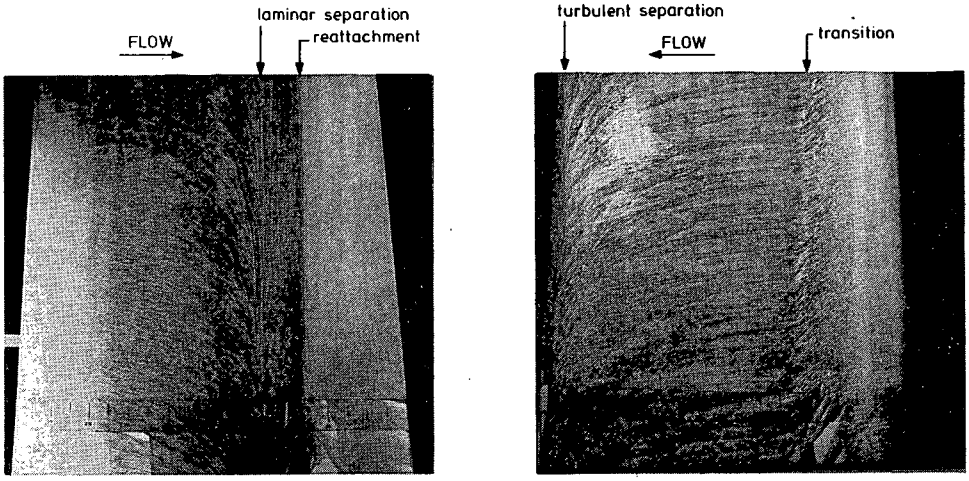

Lower surface
$\alpha = 8°$ Re = $0.85 * 10^6$

Upper surface
$\alpha = 8°$ Re = $0.85 * 10^6$

Fig. 6: Oil-flow patterns on outer wing test segment.

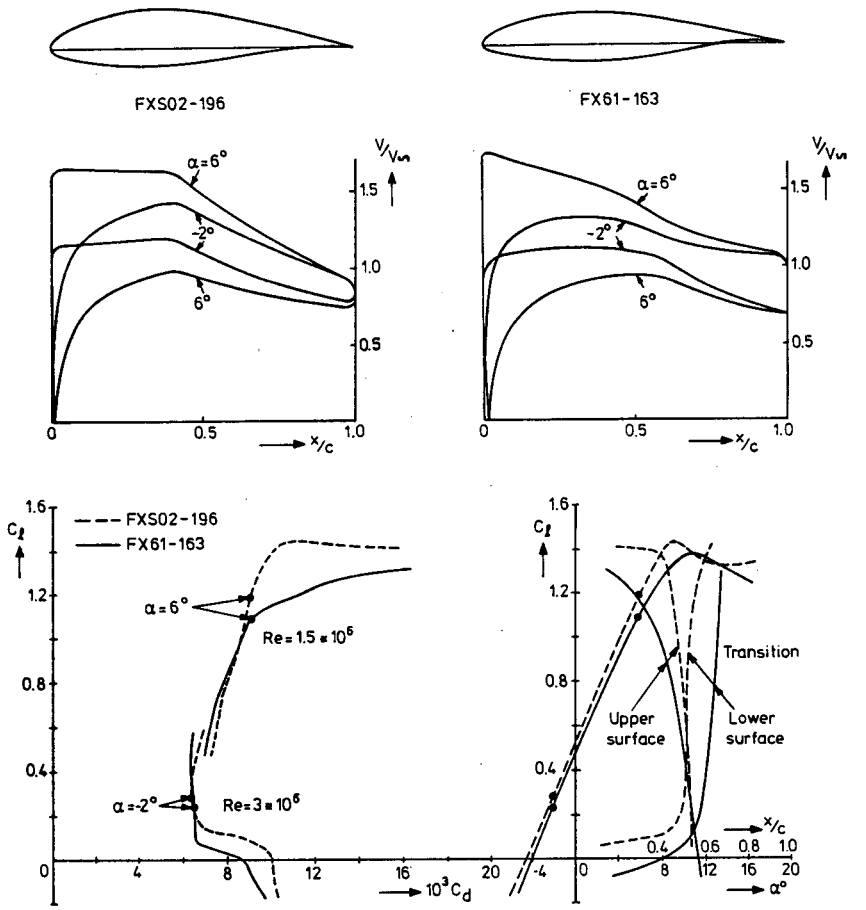

Fig. 7: Comparison of some typical airfoil characteristics.
Measurements: Stuttgarter Laminarwindkanal, Ref. 3.

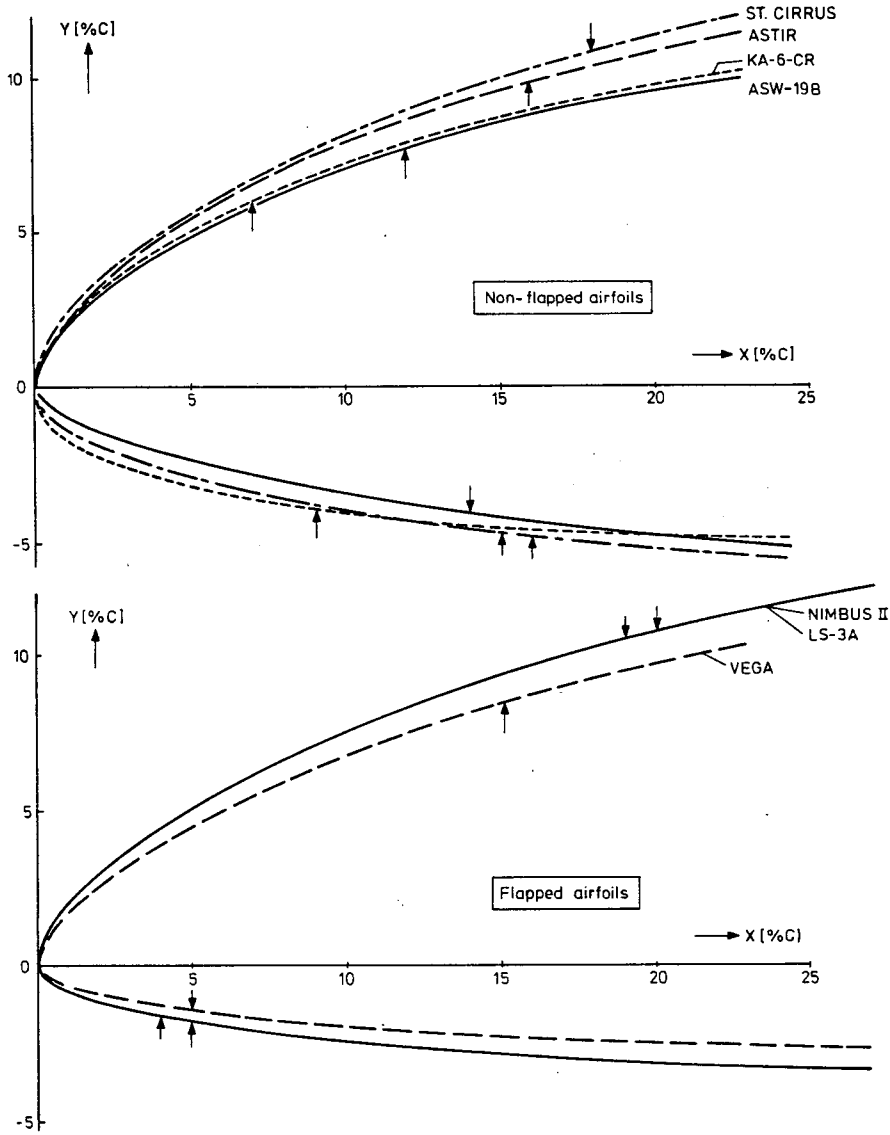

Fig. 8: Extent of insect impact pattern on some flapped and non-flapped airfoils.

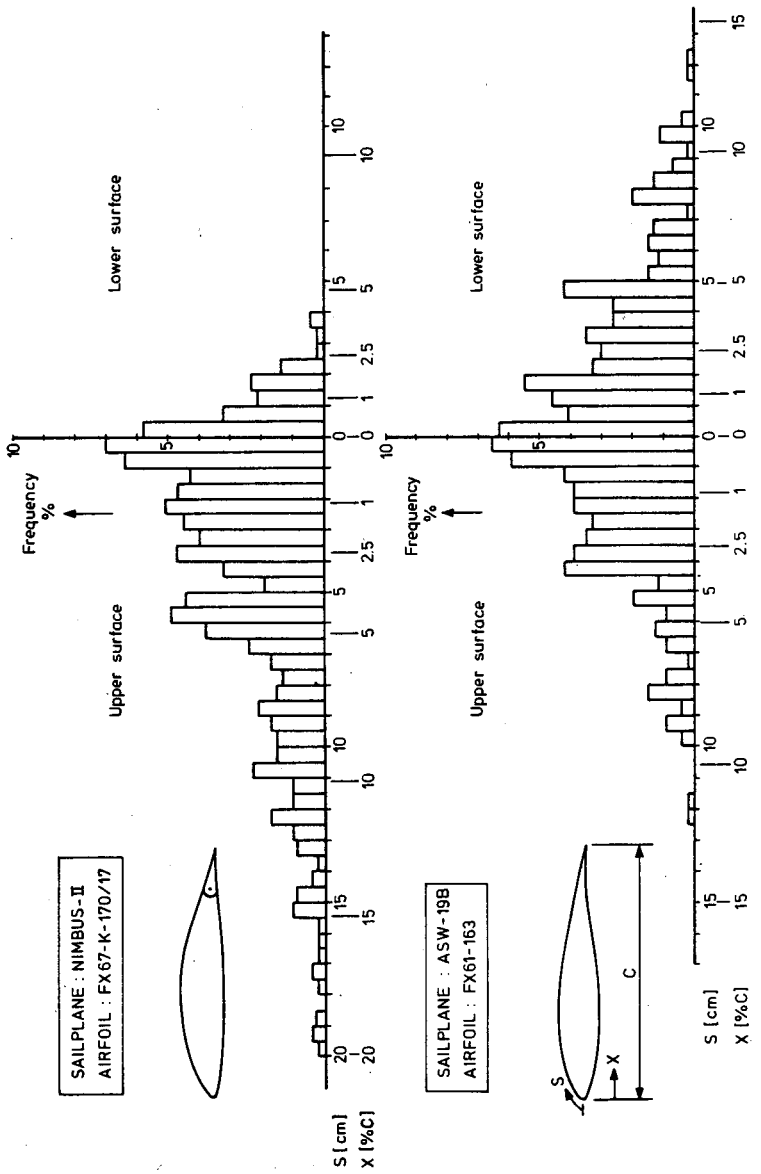

Fig. 9: Insect impact distribution on a flapped and a non-flapped airfoil.

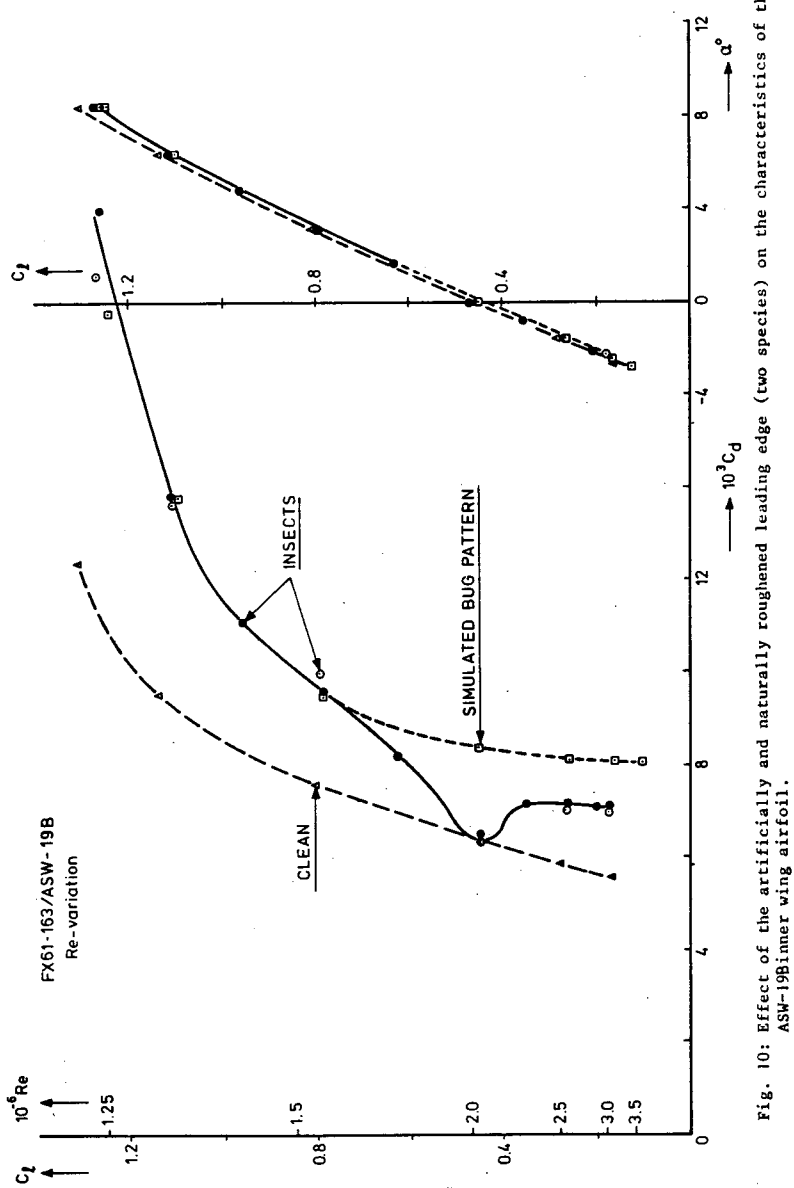

Fig. 10: Effect of the artificially and naturally roughened leading edge (two species) on the characteristics of the ASW-19Binner wing airfoil.

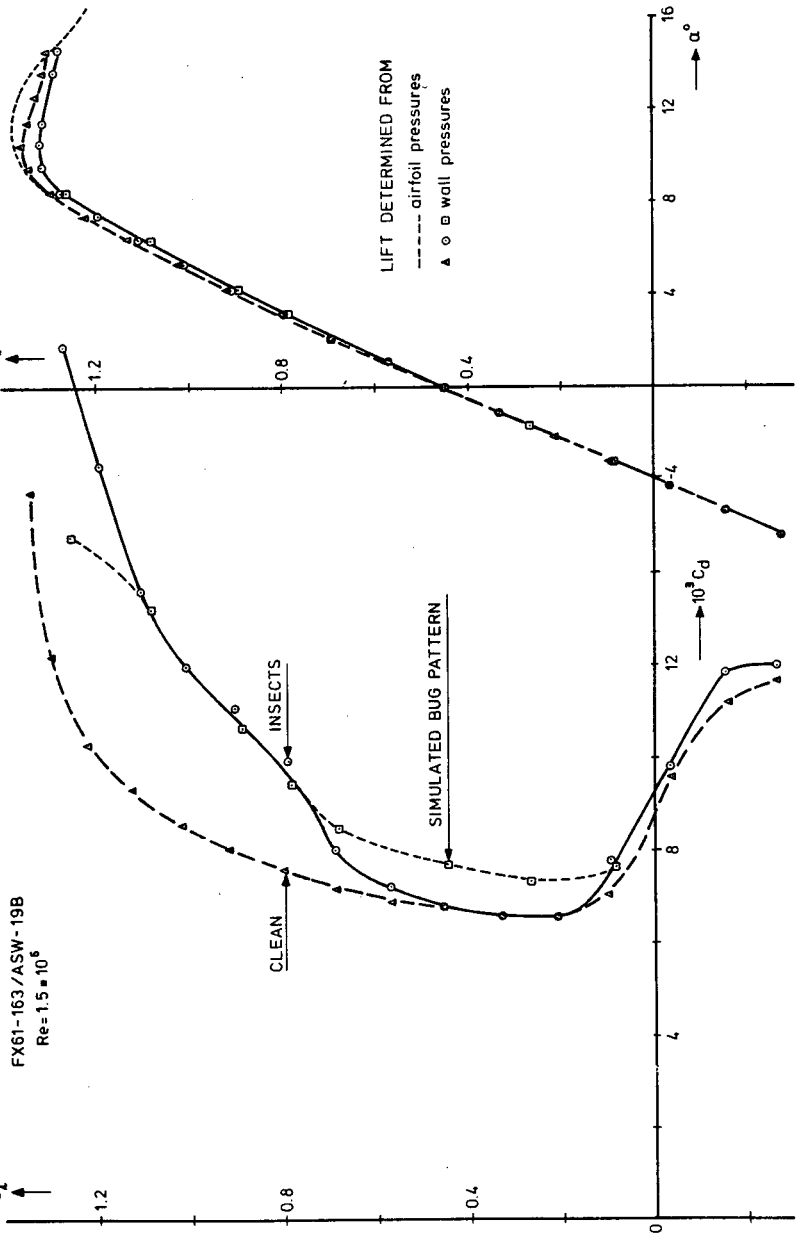

Fig. 11: Effect of the artificially and naturally roughened leading edge on the characteristics of the ASW-19B inner wing airfoil. Re = $1.5 * 10^6$.

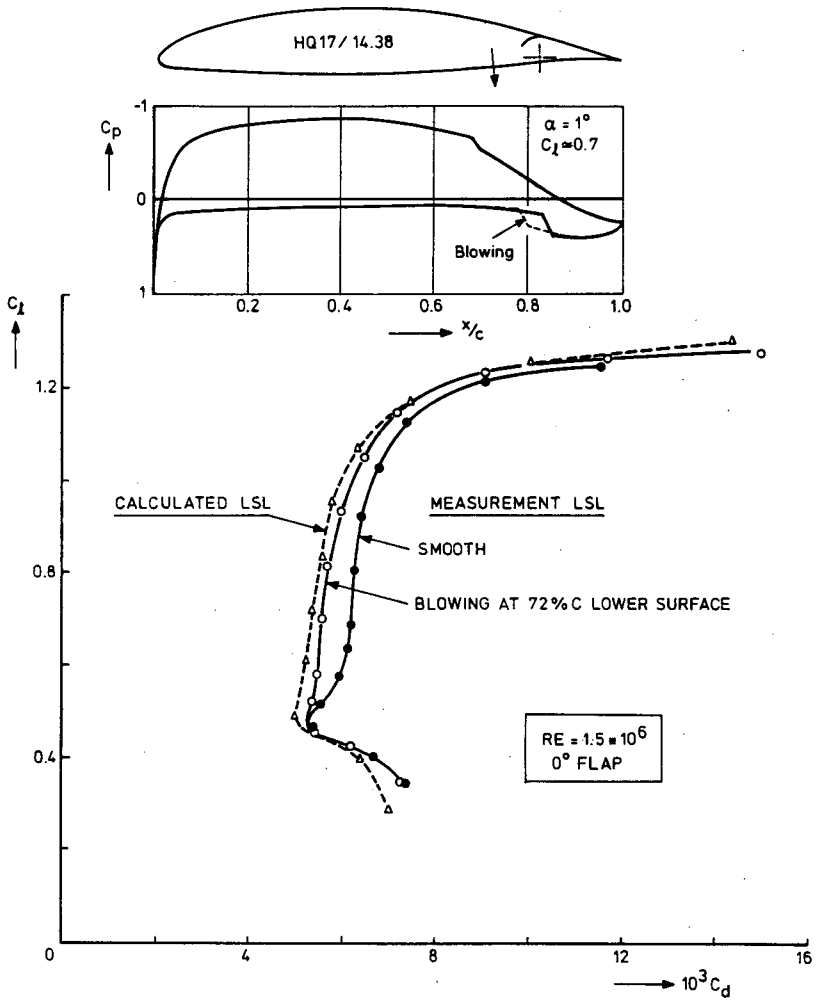

Fig. 12: Measured and calculated characteristics of HQ17/14.38.

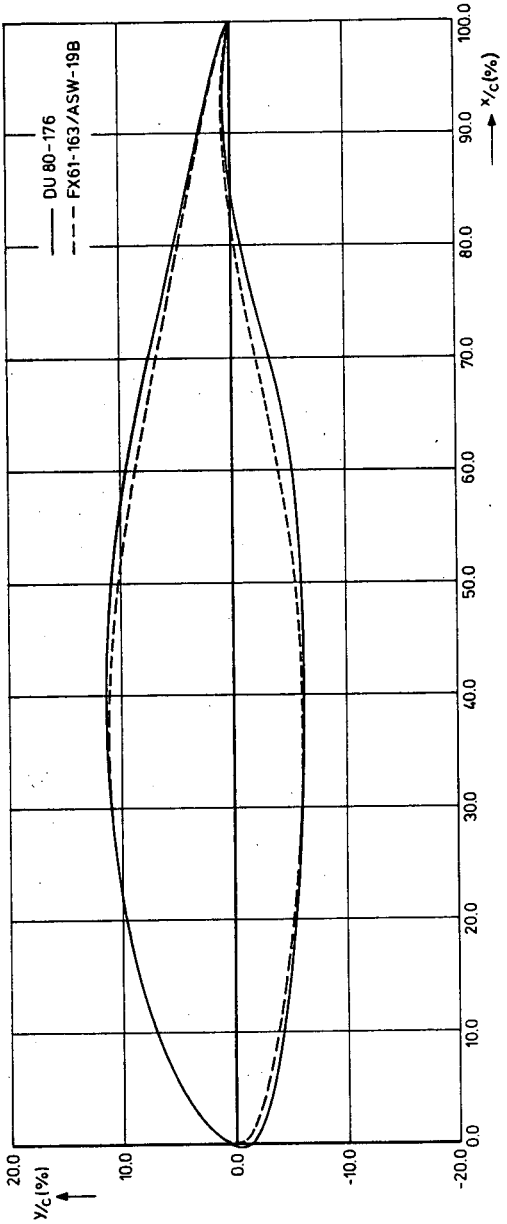

Fig. 13: The new airfoil fitted to the airfoil of the inner wing test segment.

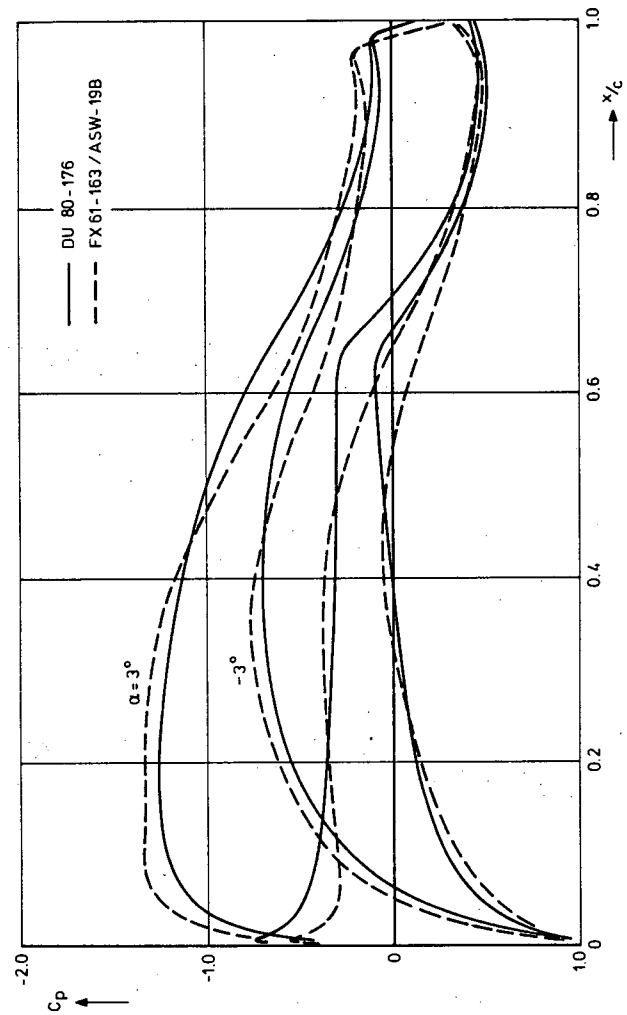

Fig. 14: Comparison of potential flow pressure distributions.

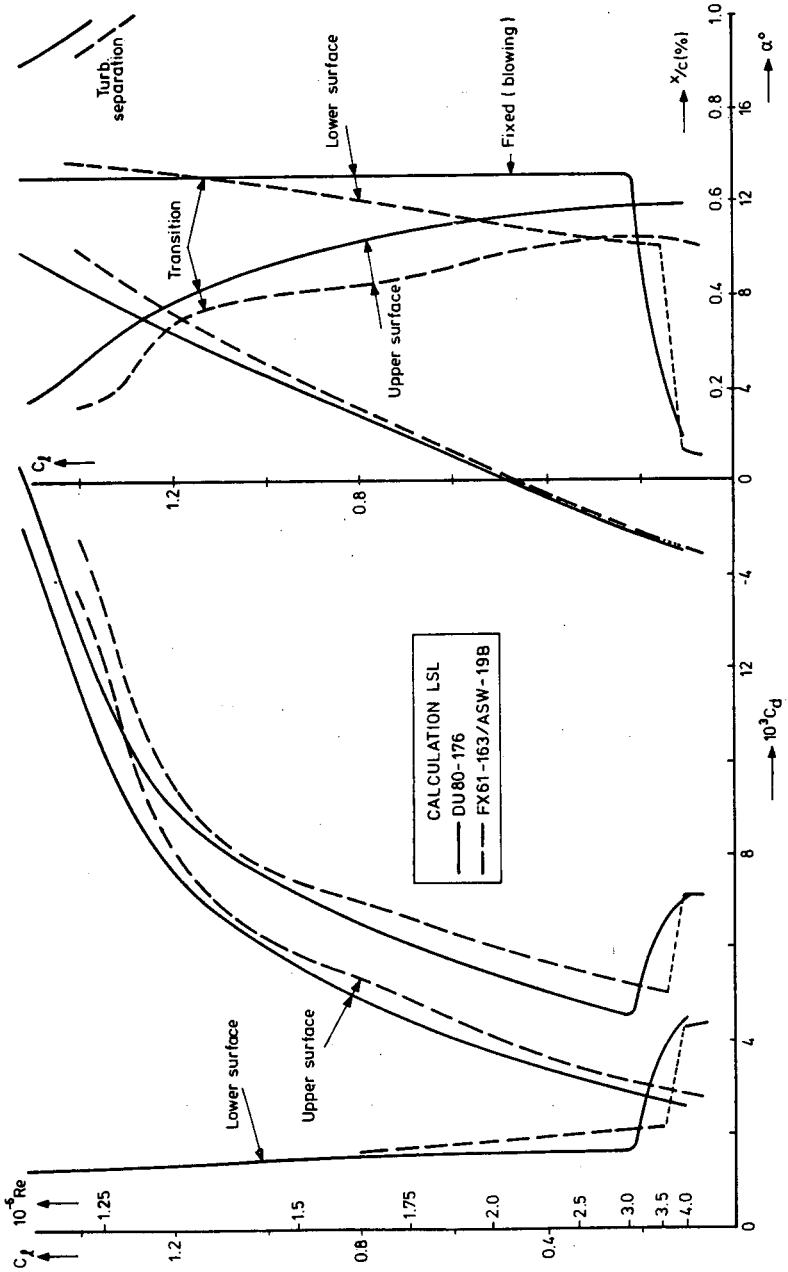

Fig. 15: Comparison of calculated characteristics.

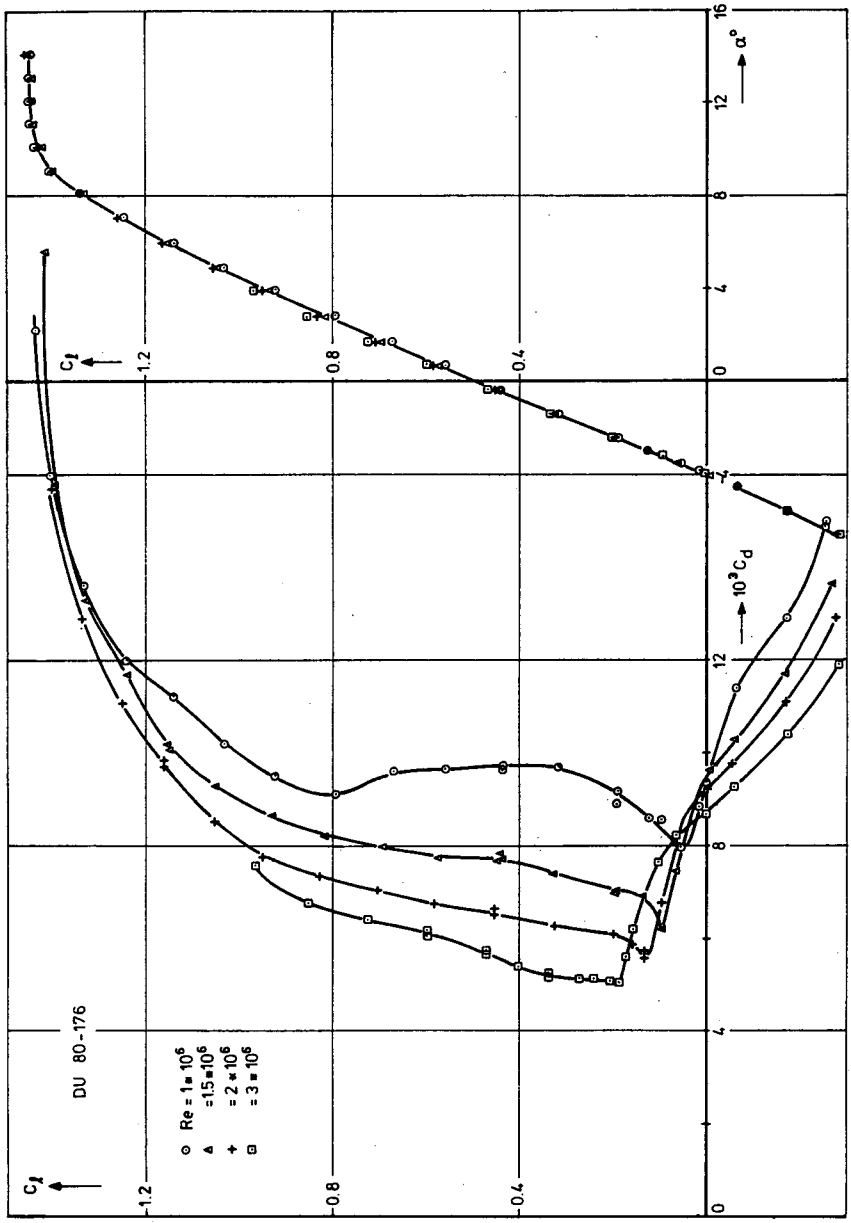

Fig. 16: Measured aerodynamic characteristics of DU80-176.

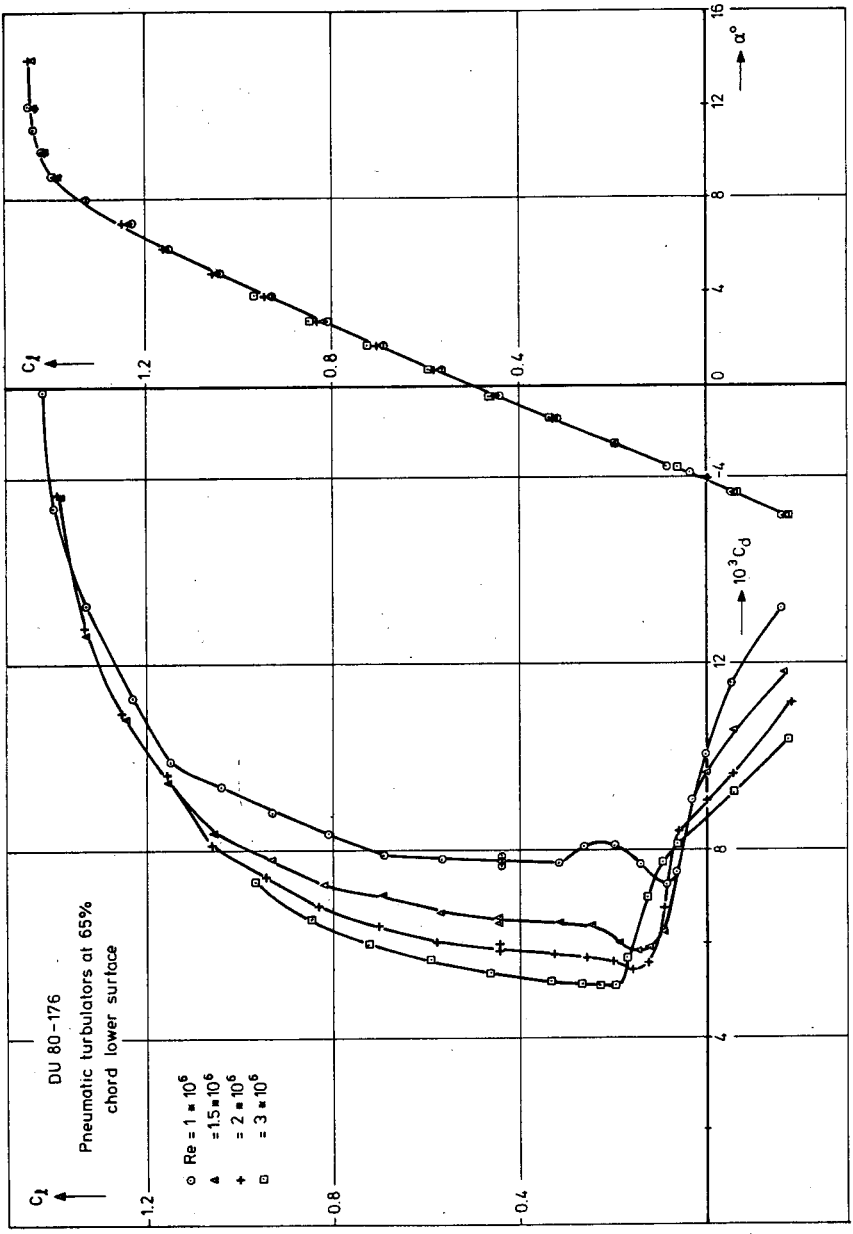

Fig. 17: Measured aerodynamic characteristics of DU80-176 with pneumatic turbulators.

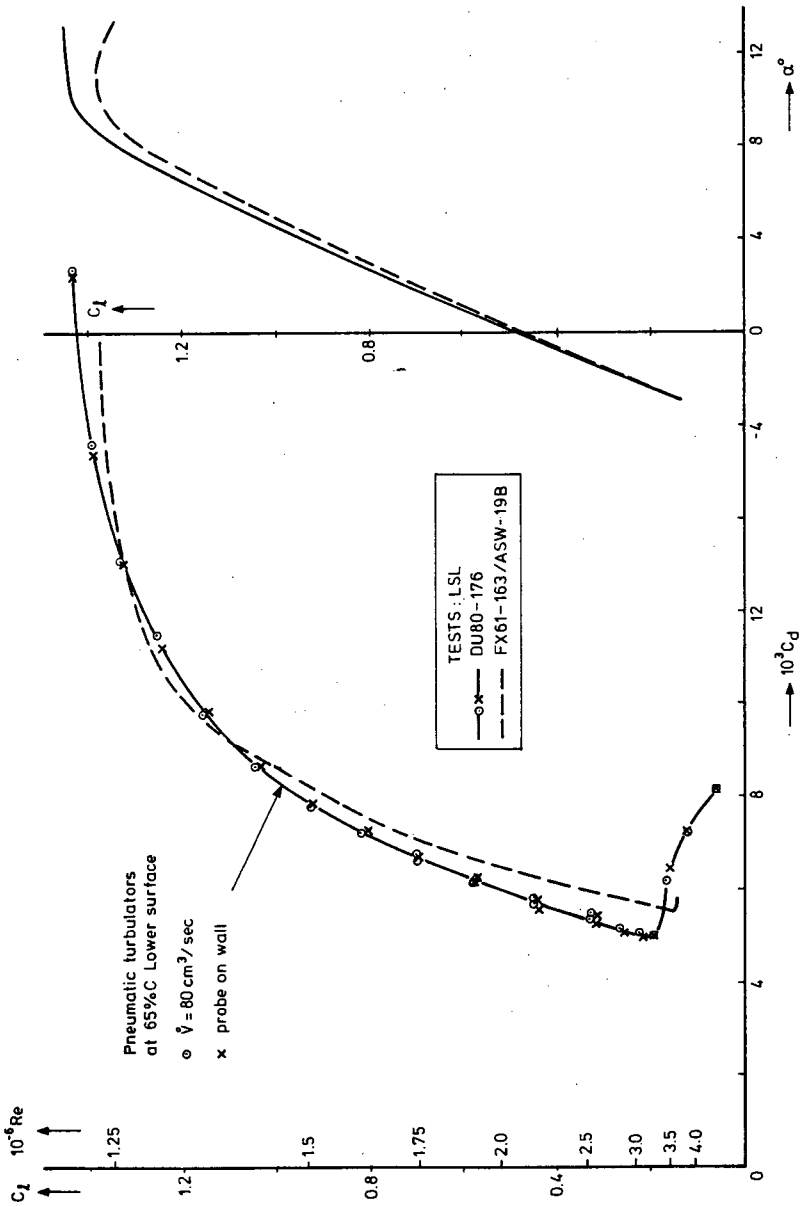

Fig. 18: Comparison of measured characteristics.

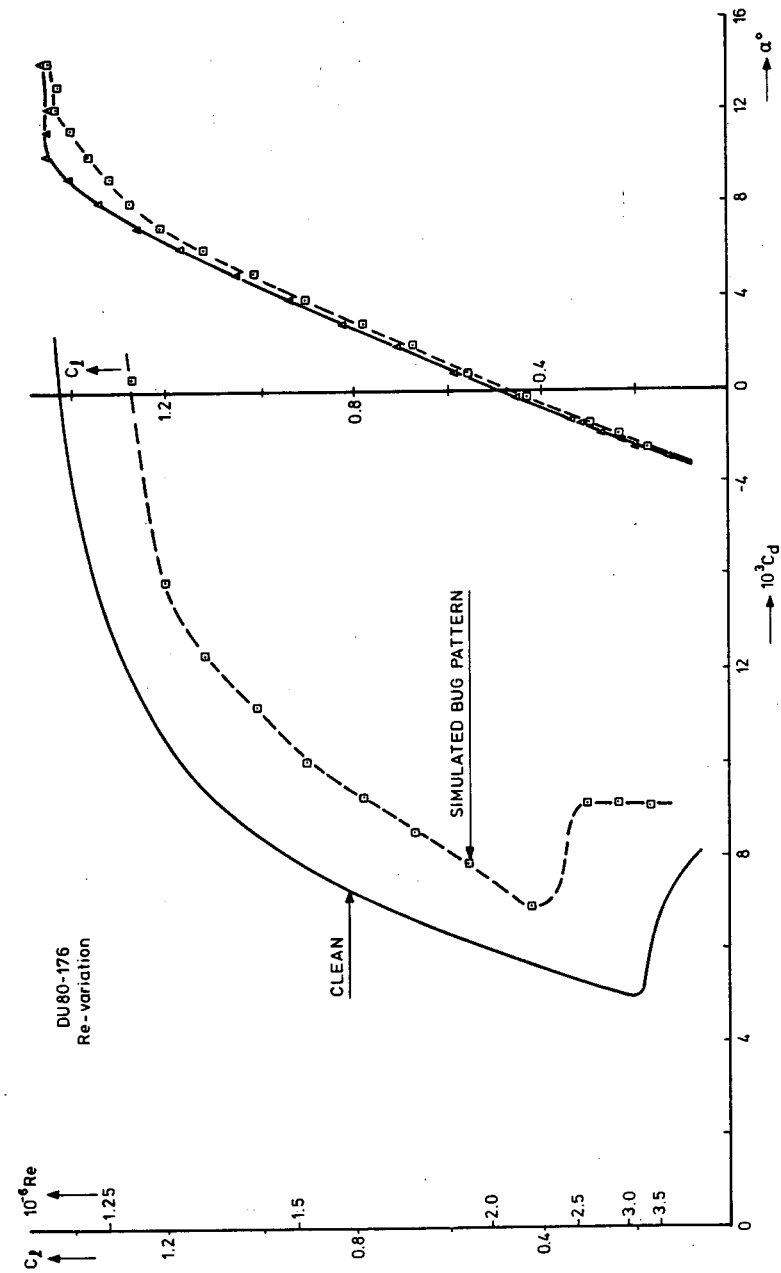

Fig. 19: Effect of the artificially roughened leading edge on the characteristics of airfoil DU80-176.

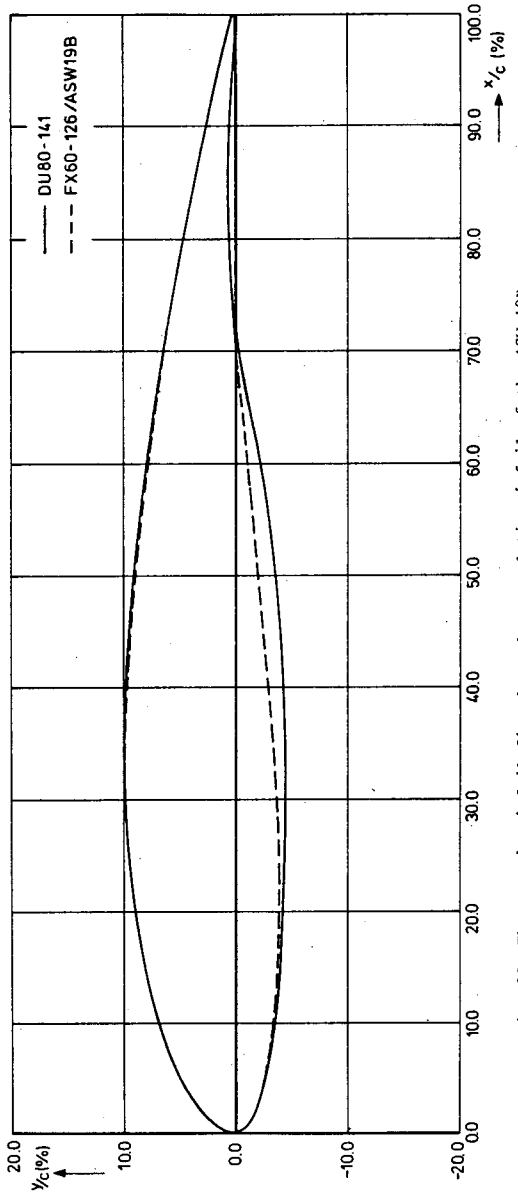

Fig. 20: The new tip airfoil fitted to the actual tip airfoil of the ASW-19B.

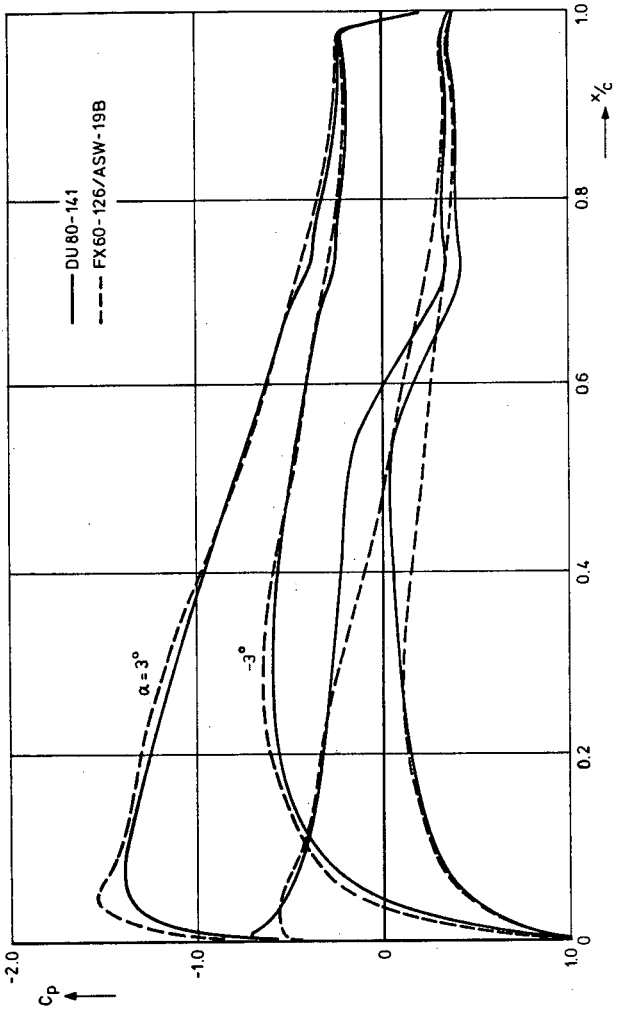

Fig. 21: Comparison of potential flow pressure distributions.

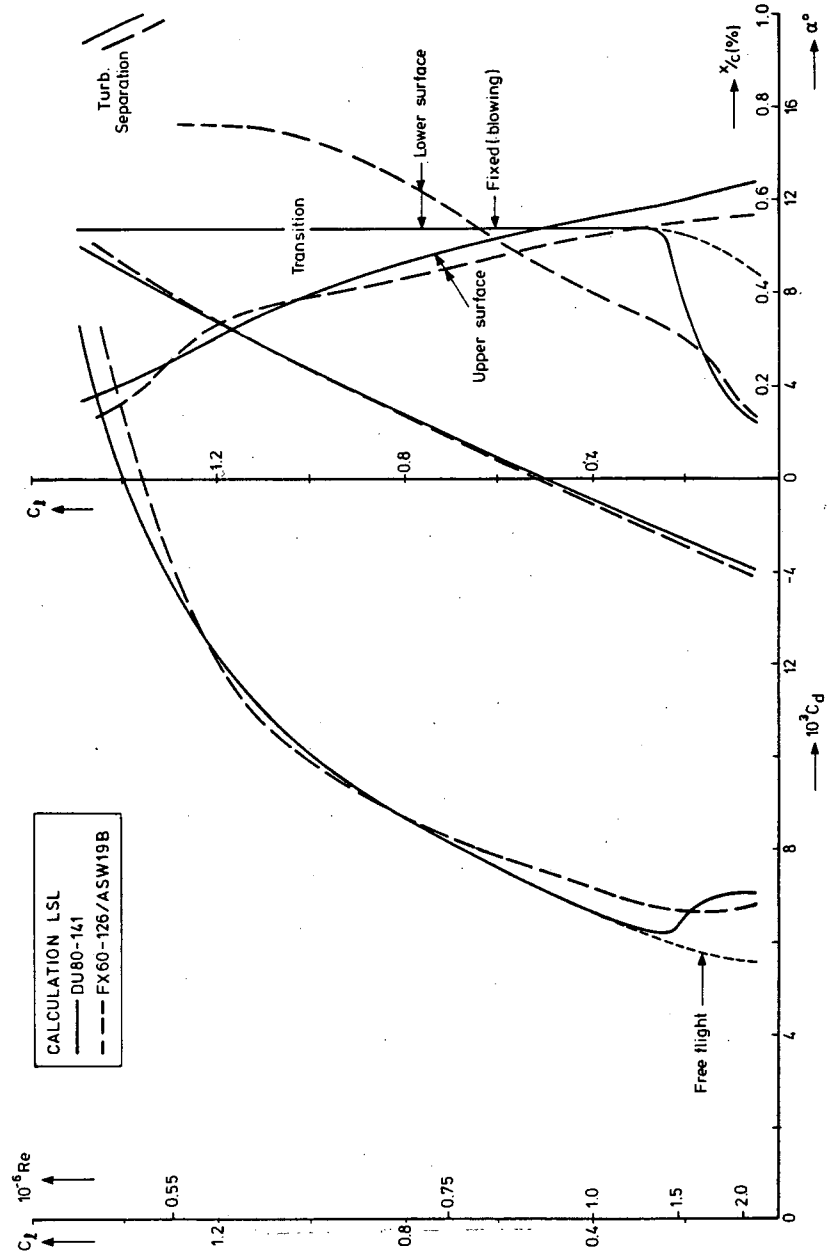

Fig. 22: Comparison of calculated characteristics for the tip airfoils.

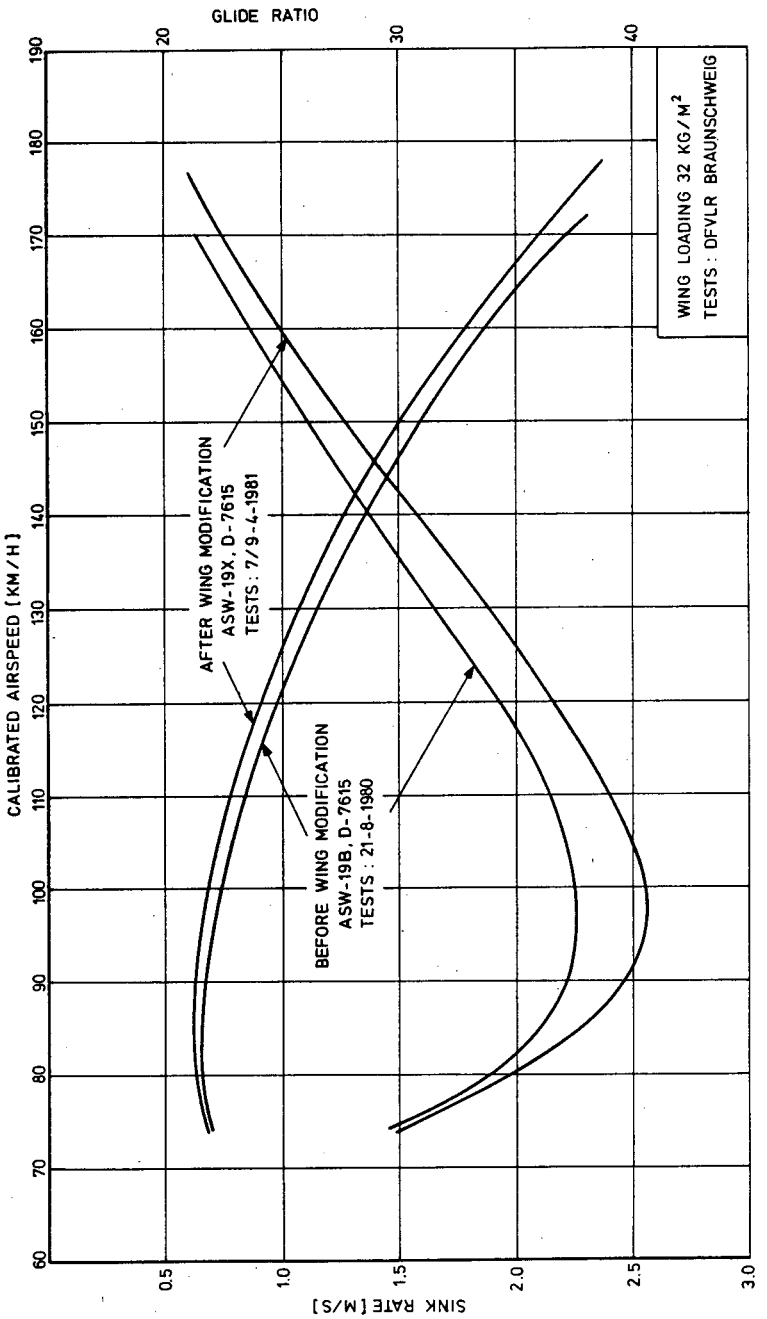

Fig. 23: Measured flight performance polars, before and after the wing modification.